Fuel-Air Mixing In A Turbulent Coannular Pipe Flow Measured Using Laser Absorption With Genetic Algorithm-Based Tomographic Reconstruction And Modeled With LES

J.W. Girard[1*], J.-Y. Chen[1], R.W. Dibble[1],
J. Janicka[2], and R. Homma[3]

[1]University of California, Berkeley, 50B Hesse Hall, Berkeley, CA 94720, USA
[2]Institute of Energy- and Powerplant-Technology, Technical University of Darmstadt, Germany
[3]Tokyo Gas Co., Ltd.,16-25 Shibaura, 1-Chome, Minato-ku, Tokyo, Japan, 105-0023

Abstract

This research aims at improving the knowledge base of fuel-air mixing through measurements and modeling. The measurements are from an improved tomographic reconstruction method that is relatively easy to accomplish. A novel aspect of this research is the use of tomography for generating the RMS of fuel concentration. Measurements of fuel concentration for a mixing field were tomographically reconstructed from time resolved line of sight laser absorption measurements.

The modeling is done using large eddy simulations (LES). LES predictions were compared to measurements of the mean and RMS of fuel concentration. The LES model predicted time-averaged radial fuel concentration profiles to within 5%, and overpredicted the RMS of fuel concentration slightly, predicting the trends correctly.

Nomenclature

1-D	1-Dimensional
2-D	2-Dimensional
3-D	3-Dimensional
CAT	Computer Aided Tomography
CO	Carbon Monoxide
d	Diameter of Smaller (Inner) Pipe in Experiment
D	Diameter of Larger (Outer) Pipe in Experiment
$D_{i,j}$	Distance between grids i and j
D_{outer}	Diameter of Larger (Outer) Pipe in Experiment
DNS	Direct Numerical Simulation
G	Girard Factor, Length Scale Near the Taylor Scale, the Distance at Which Correlations Become Substantial
GA	Genetic Algorithm
HC	Hydrocarbon
I	Intensity of Laser Radiation
I_o	Initial (Un-Attenuated) Laser Radiation Intensity
IR	Infrared
K	Kelvin Temperature Scale
ℓ	Length Coordinate Along Laser Beam Path
L	Pathlength of Absorption
LES	Large Eddy Simulation
ln	Natural Log
LOS	Line-of-Sight
LPM	Lean Premixed
NO	Nitric Oxide
NO_x	Oxides of Nitrogen
O_2	Oxygen
P	Projection
P*	Pressure
ppm	Parts Per Million
r	Radial Distance from the Center of the Pipe
R	Radius of Larger (Outer) Pipe in Experiment
Re	Reynolds Number
RANS	Reynolds Averaged Navier Stokes
RFA	Real-Time Fuel-Air Analyzer
RMS	Root Mean Square
t	Time
V_{outer}	Velocity of Outer Pipe Flow
x	Axial Distance From Exit of Fuel Pipe in Experiment
X	Fuel Mole Fraction, or Fuel Concentration
X_{CH4}	Fuel Mole Fraction, or Fuel Concentration
X_i	Averaged Fuel Mole Fraction Over Segment i
X_{RMS}	Fuel Mole Fraction RMS, or Fuel Concentration RMS
z	Tangential Distance from Center of Pipe
α	Absorption Coefficient
$\Delta\ell$	Path length Across a Small Segment
v	Kinematic Viscosity

* Corresponding author. E-mail: james.girard@a1.net

Introduction

Many practical combustion devices premix fuel into air to lean conditions prior to combustion. Such devices include spark ignited piston engines and lean premixed (LPM) gas turbine combustors. In order for a LPM combustor to effectively reduce NO_x levels, the air and fuel should be well mixed prior to the combustion event (Fric, 1993 [1], Graham and McKindley, 1991 [2]). A well mixed system is characterized by a mean fuel concentration, that is lean, with a small temporal and spatial root mean square (RMS) value about the mean.

Inadequate fuel-air mixing can have the same mean, but has a larger RMS such that, occasionally, combustion may take place at near-stoichiometric air-fuel ratios at some time, while at other times the mixture is temporarily too lean and will not burn. The sporadic combustion at near-stoichiometric air-fuel ratios has higher than average temperatures. These high temperatures lead to very high NO_x levels due to the well known exponential temperature dependence of the production rates of NO_x (Warnatz et al., 2001 [3]).

Poor mixing of the fuel and air has other negative effects in addition to the increase in NO_x emissions for lean premixed combustion systems. The incomplete combustion at locations where the air-fuel ratio is very lean may result in high levels of hydrocarbon (HC) and carbon monoxide (CO) emissions. Additionally, LPM combustors are prone to high pressure oscillations, and it has been shown that the concentration of the fuel in air correlates with these oscillations in combustor pressure (Girard et al., 2001 [4], Mongia et al., 1998 [5]). Thus, in the design of a lean premixed gas turbine, it is essential that the mixing of fuel into air is well characterized; minimally one needs a mean and RMS of fuel concentration.

The goal of the current research is the improvement of the knowledge base of fuel-air mixing through: 1) a rugged easy-to-use optical line of sight (LOS) absorption technique, 2) an associated reconstruction software, and 3) computational fluid dynamic modeling using the technique of large eddy simulations (LES). In this paper we study the ability of generating both the mean and RMS of fuel concentration, at the exit of a premixer, from measurements obtained using a robust LOS laser absorption technique. Additionally, the performance of LES for a simplified geometry as a step toward application of LES modeling to an actual lean premixed combustor is studied.

For the current research we use experimental measurements of mean and RMS of fuel concentration for characterizations of the performance of the LES model. As a future goal we imagine the simple but powerful diagnostic, that of reconstructing the RMS and mean concentration from LOS measurements, can be easily used for studies of gas turbine premixers.

Tomographic reconstruction has become a powerful diagnostic tool since Hounsfield and Cormack shared the 1979 Nobel Prize for Medicine for the development of Computer Assisted Tomography. In addition to the common use of tomography for steady state fuel concentration measurements, Faris (1986 [8]) has demonstrated that tomography can also be used to relate the deflection of a laser beam to fluid flow characteristics. Carey et al. (1999 [9]) used near infrared (IR) absorption tomography to determine the spatial distribution of chemical species in a running internal combustion engine. More details on the principles of tomography can be found in Bertrero and Coccacci (1998 [10]) and in Williams and Beck (1995 [11]).

The important aspects of the current research are that the genetic algorithm (GA) method has the potential of reconstructing a non symmetric concentration field with reasonable accuracy from a limited number of experimental measurements, and that we apply the GA technique to reconstruct the RMS of the concentration profile. The research described in this paper consists of: 1) formulating the problem of tomographic reconstruction of time-average mean and RMS radial concentration profiles in such a way as to be optimized by a GA, 2) applying this technique to some numerical "test cases" for validation, then 3) using it on data from a turbulent coannular pipe flow, thus assessing the ability of an LES model to reproduce the measured fuel-air mixing spatially and temporally.

Experimental Setup/Procedure

In numerical simulation of fluid mechanics, such as Reynolds Averaged Navier-Stokes (RANS), time-resolved details are not predicted. Time-resolved details are predicted by direct numerical simulation (DNS). However, due to the vast computational effort involved, DNS is usually only applied to simple flows within a very small domain. LES models are truncated (more accurately: filtered) DNS models (Pope, 2000 [12]) that use coarser grids than DNS and then have subgrid models for small-scale turbulence, as a means of reducing the computational costs relative to DNS (see, for example Branley and Jones, 2001 [13]). LES gives time resolution in a 3-D simulation, unlike most combustion models, but requires much more computer resources than RANS. Table 1 gives the input and grid parameters of the current LES. Details of the LES can be

found in the thesis of Forkel (1999 [14]), Forkel et al. (1999 [15]), and Kemp et al. (2001 [16]), with details on the subgrid scale model being available in Germano et al. (1991 [17]).

Table 1
Details of large eddy simulation (LES) software model used

Grid System	Non-uniform in radial direction, clustered grids near central pipe
Grid Size	128x64x47 ($x = 2D_{outer}$, $\Theta = 360^o$, $R = D_{outer}/2$)
Accuracy	Fourth-Order in Space, Third-Order in Time
Subgrid Turbulence Model	Germano Dynamics
Inlet Flow Boundary Conditions	Stored time serial results from a separate3-D LES for fully developed coannular pipe flow
Wall Treatment	Wall Function
Time Steps for Statistically Stationary State	50,000
Typical CPU Time	~ 3 days on Alpha Dec 500 au

A coannular pipe flow experiment was constructed, consisting of a center pipe flow of fuel, surrounded by a pipe flow of air, for evaluation of the LES mixing model performance. Figure 1 gives a schematic of the setup. The diameter of the outer pipe is D = 7.6 cm, while that of the inner pipe is d = 6.4 mm. Thus the diameter ratio of the pipe flow setup is d/D = 0.084. The center fuel pipe is 3.3 meters in length, while the air pipe length varied from 3.3 to 3.5 meters. The long air pipe (over 40 diameters) suggests that there was a fully developed coannular pipe flow given that the Reynolds number was approximately 10^5 based on the outer pipe (White, 1994 [18]).

LOS Laser absorption measurements were made at the exit of the outer (air) pipe (see Fig. 1). In this way measurements at different axial distances from the center (fuel) pipe exit were accomplished by changing the length of the outer pipe while keeping the position of the inner pipe fixed. Axial distance from the center pipe exit will be referred to as small x, and x/d will refer to the axial distance normalized by the diameter of the center pipe. Measurements of the fuel concentration were obtained by the use of a 3.392 μm wavelength He-Ne Laser. Many hydrocarbons absorb radiation at this wavelength. Beer's law can be used in relating the amount of light absorption to the concentration of fuel (see, e.g. Lee et al. 2000 [19], Yoshiyama et al. 1996 [20], Perrin et al., 1989 [21], Mongia 1998 [22], or Ebert et al. 2000 [23]). At standard temperature and pressure, the absorption of laser light by a concentration of molecules follows Beer's Law:

$$\frac{dI}{d\ell} = -I \cdot \alpha \cdot P^* \cdot X_{CH_4}(\ell) \tag{1}$$

where I denotes intensity of laser radiation, α the absorption coefficient for given fuel ($cm^{-1}\,atm^{-1}$), P^* the pressure (atm), ℓ the coordinate along laser beam path (cm), and $X_{CH_4}(\ell)$ the fuel mole fraction, dependent on position ℓ and time t.

Integration of Eq. (1) with α being constant yields

$$\int \frac{dI}{I} = -\alpha \cdot P^* \cdot \int X_{CH_4}(\ell) \cdot d\ell \tag{2}$$

$$\ln(I/I_o) = -\alpha \cdot P^* \cdot \int X_{CH_4}(\ell) \cdot d\ell \tag{3}$$

where I_o is the initial (un-attenuated) laser radiation intensity. For a perfectly mixed system, where the concentration is constant across the measurement length, one obtains

$$X_{CH_4} = -\frac{\ln(I/I_o)}{(\alpha \cdot P^* \cdot L)} \tag{4}$$

where L is the path length of absorption (cm). The absorption coefficient α is dependent on temperature, pressure, and the type of fuel being characterized. The absorption coefficient for methane was measured by Perrin et al. (1989 [21]) as approximately α = 10 $cm^{-1}atm^{-1}$ at standard temperature and pressure. As can be seen from Eq. (3), laser absorption measurements give an integrated fuel concentration over the path of the laser beam. In our application, the laser beam passed across the pipe exit, at the same orientation, at various cords as shown in Fig. 1. For this system, the concentration across the pathlength of laser absorption is not constant, so that Eq. (4) cannot be used directly (only directly applicable when the concentration is constant across the path). A tomographic reconstruction algorithm was used for generating a radial profile of concentration from the laser beam absorption data. Several routes can be taken for tomographic reconstruction: 1) Abel inversion (Abel, 1826 [24]), 2) Fourier deconvolution (Dasch, 1996 [25], Ravichandran and Gouldin, 1998 [26]), 3) filtered backprojections (Jain, 1989 [27]), 4) genetic algorithm, GA, (Kihm and Lyons, 1996 [28]) and 5) variational approach (Kybic et al.,

2001 [29]). For this research we chose to employ a GA-based reconstruction scheme. A GA-based reconstruction technique was used for calculating the concentration profiles because of the ability of the technique to maximize the reconstruction accuracy from a minimal number of projections, as shown by Kihm and Lyons (1996 [28]). Details about the GA reconstruction technique will be given in the following section.

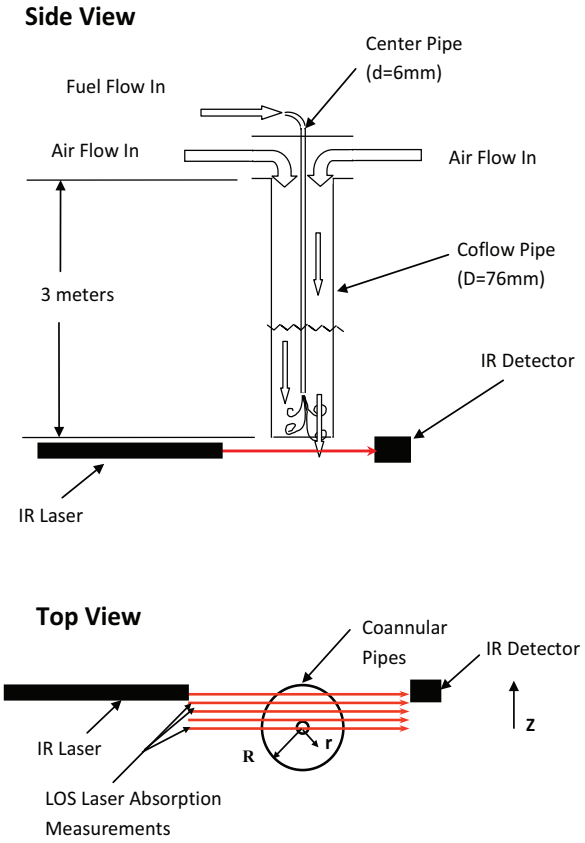

Fig. 1. Experimental setup for coannular pipe flow mixing experiment.

After demonstrating that the experimental measurement system was reasonably accurate by testing the system in laboratory experiments using known concentration profiles, radial concentration profiles were generated from LOS measurements at various downstream locations (for comparison with predictions of the LES model). Table 2 describes the experimental operating conditions at each of the sampling points.

The flow rates shown in Table 2 were set with the goal of making the outer Reynolds number (Re) as high as possible, and of matching the average velocities of the inner and outer pipe flows. The Reynolds number for the flow is defined by $\mathrm{Re} = \frac{V_{outer} \cdot D}{\nu}$, where V_{outer} is the nominal velocity of the outer pipe flow, D is the diameter of the outer pipe, and ν is the kinematic viscosity of air; we used 1.5 x 10^{-5} m^2/s (Hinze, 1975 [30]). For the experiments described in Table 2, the nominal velocities for the inner and outer pipe flows were 26 to 27 m/s (making the friction velocities for the inner and outer pipe flows around 1.6 and 1.2 m/s, respectively, as per the textbook by White, 1994 [18]).

Table 2
Test matrix for methane-air mixing experiments[a]

Axial Distance (x/d)[b]	Azimuthal Orientation (Arbitrary 0° Ref.)	Reynolds Number (Outer Flow)	Fuel Used
24	0, 90, 180 & 270	1.37 x 10^5	Methane
12	90 & 270	1.37 x 10^5	Methane
6	90 & 270	1.37 x 10^5	Methane

[a] Nominal air flow rate was 7460 slm, nominal fuel flow rate was 53 slm.
[b] x/d is the axial distance x from the end of the center (fuel) pipe divided by the center pipe diameter d.

Tomographic Reconstruction using a Genetic Algorithm

Formulation of Equations for Reconstructing the Mean Fuel Concentration Profile

In many optical measurement techniques, LOS absorption measurements are taken, then the concentration field is calculated using a tomographic reconstruction technique. Figure 2 gives a schematic of the situation of LOS absorption measurements for an axisymmetric situation.

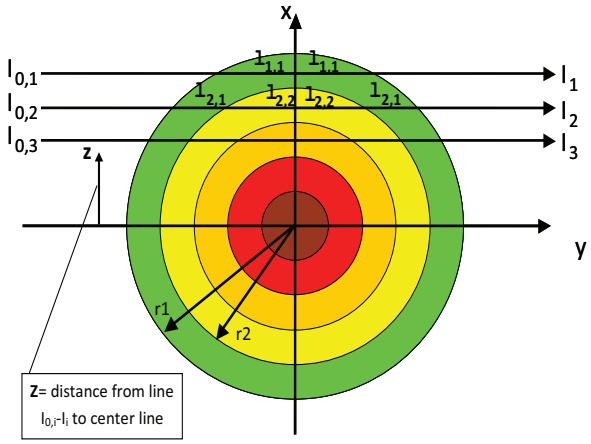

Fig. 2. Example of LOS measurements for a fuel concentration profile given a simple axisymmetric concentration field.

From Eq. (3) it is seen that if we knew the concentration profile (X_{CH4} as a function of position, r or ℓ, and time t), calculating the LOS intensity ratios would be relatively easy. Given the spatially resolved concentration values X_{CH4}, calculating the LOS intensity ratios is accomplished by breaking the path of the LOS measurement into annular segments at a small enough scale so that assuming the concentration across a segment is uniform will result in little error. Although each segment has a uniform concentration, it can change in time. Figure 3 gives a simple schematic of the situation.

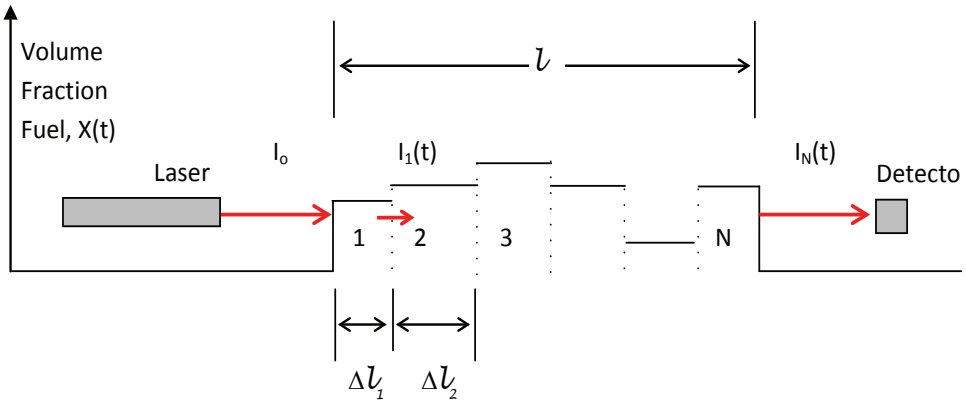

Fig. 3. 1-D system with time varying fuel concentration, sub-divided into N small segments. The concentration across a given segment is assumed to be uniform.

A relation between the RMS of the natural log of the measured signals ($I_N(t)/I_o$, from Fig. 3) and the RMS fuel concentration values ($X(t)_{RMS}$) will be developed later in this paper. Applying Beer's law to each segment shown in Fig. 3, one obtains

$$\ln\left(\frac{I_i(t)}{I_{i-1}}\right) = -\alpha \bullet P^* \bullet \Delta\ell_i \bullet X_i(t) \quad \text{i} = 1, \text{N} \qquad (5)$$

where $I_i(t)$ is the time-dependent intensity of the laser beam leaving the i-th segment, $\Delta\ell$ is the path length across the segment (cm), and $X_i(t)$ is the spatially averaged fuel volume fraction within the segment. Combining equations of the form given in Eq. (5) for each segment across the path leads to:

$$\ln\left(\frac{I_N(t)}{I_o}\right) = -\alpha \bullet P^* \bullet \sum_{i=1}^{N} \Delta\ell_i \bullet X_i(t) \qquad (6)$$

Equation 6 can be used in a tomographic reconstruction scheme relating the LOS intensity ratios to the fuel concentration profile.

Brief Description of Genetic Algorithm

A GA is a function optimization technique based on the application of genetic principles. Essentially a GA takes a set of plausible values for parameters in a function, and optimizes the values based on assigned criteria through the genetic processes of selection, crossover, and mutation (Goldberg, 1989 [31]). For the case of tomographic reconstruction of fuel concentration, the parameters that the GA optimizes are the fuel concentration values that comprise the fuel concentration profile. The criteria used for the optimization are the measured LOS intensity ratios.

The GA works as follows for the case of tomographic reconstruction of fuel concentration. The GA randomly generates a group of plausible concentration profiles; these profiles are applied to Eq. (6) and we obtain a vector of LOS intensity ratios at discrete radial locations for each of the plausible concentration profiles. The GA compares these vectors to the measured vector (laser intensity ratios for the various radial locations), and ranks each of the plausible concentration profiles based on comparisons of each of the synthetic vectors with the measured vector. The plausible concentration profiles that gave the best vector matches are retained for future generations in the GA, while poor vector matches are discarded. For each generation, several genetic type operators are applied to the set of solutions, including crossover and "mutation". Since the best fit vector is favored in consecutive generations of the GA program, the solutions generally approach the best fit to the experimental data

(Powell and Skolnick, 1993 [32]). The random mutations that we insert in the GA (at variable intervals ranging from every 10th to every 100th generation) prevent, or at least discourage, the solution from getting «stuck» in local minima. Thus, after many generations we obtain a plausible concentration profile that gives very nearly the correct intensity ratios for each of the absorption lines. Kihm and Lyons (1996 [28]) have applied a GA-based program to the case of tomographic reconstruction of a time-averaged concentration field at the exit of a coannular pipe flow (center fuel pipe exiting into co-flowing air) and found that the GA performed well with a small number of LOS measurements.

Fuel Concentration RMS Reconstruction

Formulation of Equations for Reconstructing the RMS Fuel Concentration Profile

In this section we derive the relation between the RMS of the LOS projections and the RMS fuel concentration values for a gaseous fuel-air mixing situation. The reconstruction problem examined previously is now analyzed for a case where fuel concentration is not constant in time. Consider a line of sight measurement through a concentration field (as previously shown in Fig. 3). As an approximation, the field is sub-divided into several segments, with the concentration across a given segment assumed to be uniform.

For simplicity, define a projection, P (not to be confused with pressure P^*), such that Eq. (6) can be rewritten as

$$P(t) = \frac{\ln\left(\frac{I_N(t)}{I_o}\right)}{\alpha \bullet P^*} = -\sum_{i=1}^{N} \Delta\ell_i \bullet X_i(t) \qquad (7)$$

This equation describes the relation between the natural log of the intensity ratio (projection) for a given absorption line and the concentration field. Thus the natural log of the intensity ratio, $\ln(I/I_o)$, is a linear function of the time-dependent concentrations of each radial position. From Eq. (7) we can develop a relation between the RMS of $\ln(I/I_o)$ and the RMS of the fuel concentrations. The first step is to decompose each term of Eq. (7) into a mean and a fluctuating component leading to

$$\overline{P} + P' = -\sum_{i=1}^{N} \Delta\ell_i \bullet \left(\overline{X_i} + X_i'\right) \text{ or } P' = -\overline{P} - \sum_{i=1}^{N} \Delta\ell_i \bullet \left(\overline{X_i} + X_i'\right) \qquad (8)$$

Second, to solve for the RMS of P, we square both sides of the equation and average

$$\overline{P'^2} = \overline{\left[\overline{P} + \sum_{i=1}^{N} \Delta\ell_i \bullet \left(\overline{X_i} + X_i'\right)\right]^2} \qquad (9)$$

Expansion of the right hand side of Eq. (9) leads to

$$\overline{\left[\ln\left(\frac{I_N}{I_o}\right)\right]'^2} = \alpha^2 \bullet P^{*2} \bullet \sum_{i=1}^{N} \Delta\ell_i^{\,2} \bullet \overline{X_i'^2} + \alpha^2 \bullet P^{*2} \bullet \sum_{i=1}^{N} \sum_{j=1, i\neq j}^{N} \Delta\ell_i \bullet \Delta\ell_j \bullet \left(\overline{X_i' \bullet X_j'}\right) \qquad (10)$$

The terms X_i and X_j in the above equations correspond to the fuel concentration values at two different locations in the system, i and j. Details of this derivation can be found in the Doctoral Thesis by Girard (2003 [33]).

For the case where the concentration fluctuations in the individual segments have no correlation, the correlation terms, $\overline{X_i' \bullet X_j'}$, are simply zero, and Eq. (10) becomes

$$\overline{\left[\ln\left(\frac{I_N}{I_o}\right)\right]'^2} = \alpha^2 \bullet P^{*2} \bullet \sum_{i=1}^{N} \Delta\ell_i^{\,2} \bullet \overline{X_i'^2} \qquad (11)$$

If $\overline{X_i'^2}$ = constant and $\Delta\ell_i = L/N$, where L is the path length of absorption, Eq. (11) becomes

$$\overline{P'^2} = \overline{\left[\ln\left(\frac{I_N}{I_o}\right)\right]'^2} = \alpha^2 \bullet P^{*2} \bullet L^2 \bullet \frac{\overline{X_i'^2}}{N} \qquad (12)$$

This equation shows that $\overline{P'^2}$ decreases with an increase in the total number of grids if there is no correlation between segments. Although Eq. (12) is derived under special conditions, the deceasing tendency of $\overline{P'^2}$ with increasing N is expected in the general case because the fluctuations in segments along the projection would tend to cancel each other out as the number of grids N increases. With $\overline{P'^2}$ measured by LOS, the RMS can be estimated, by using Eq. (12) if one assumes no correlation, as

$$\overline{X_i'^2} = \frac{\overline{P'^2} \bullet N}{(\alpha^2 \bullet P^{*2} \bullet L^2)} \qquad (13)$$

Consequently, the estimated RMS increases with the total number of grids.

Next Eq. (10) is examined for the other extreme case, where fluctuations of concentrations in the segments are completely correlated, i.e., $\overline{X_i' \bullet X_j'} = \overline{X_i'^2}$ leading to

$$\overline{\left[\ln\left(\frac{I_N}{I_o}\right)\right]'^2} = \underbrace{\alpha^2 \bullet P^{*2} \bullet \sum_{i=1}^{N} \Delta\ell_i{}^2 \bullet \overline{X_i'^2}}_{\text{Same as equation 12}} + \underbrace{\alpha^2 \bullet P^{*2} \bullet \sum_{i=1}^{N} \sum_{j=1, i\neq j}^{N} \Delta\ell_i \bullet \Delta\ell_j \bullet \overline{X_i'^2}}_{\text{Correlation Term}} \qquad (14)$$

As can be seen from Eq. (14), the case of complete correlation is equal to the equation for no correlation Eq. (11) plus the correlation term. The $\overline{X_i'^2}$ term is positive, and therefore the RMS of projections, $\overline{P'^2}$, for the case of complete correlation will be greater than or equal to the case of no correlation. Equation 14 can be further simplified to

$$\overline{\left[\ln\left(\frac{I_N}{I_o}\right)\right]'^2} = \alpha^2 \bullet P^{*2} \bullet \sum_{i=1}^{N} \sum_{j=1}^{N} \Delta\ell_i \bullet \Delta\ell_j \bullet \overline{X_i'^2} \qquad (15)$$

Equation 15 is the relation for completely correlated fluctuations. Under the special case of $\overline{X_i'^2}$ = constant and $\Delta\ell_i = L/N$, Eq. (15) reduces to

$$\overline{\left[\ln\left(\frac{I_N}{I_o}\right)\right]'^2} = \alpha^2 \bullet P^{*2} \bullet L^2 \bullet \overline{X_i'^2} \qquad (16)$$

which is independent of the size of grids in contrast to Eq. (13) for no correlation in the fluctuations. This grid topic will be discussed further in Section 4.2.

In reconstructing the RMS concentration profile from time dependent LOS measurements, the mean concentration of the system must be such that the amount of laser radiation absorbed is neither too high, where the measured value, ≈ 0, is too close to $I_N/I_o = 0$, nor too low, where the measured value, ≈ 1, is too close to $I_N/I_o = 1$. When In/Io is too close to zero or to one, the noise in the measurements can influence the measured RMS of the projections. The acceptable amount of laser light absorbed is dependent on the amount of noise in the measurement system.

An additional source of uncertainty that must be considered is the effect of the finite laser beam diameter. The discussion thus far has considered only the case where the laser beam diameter was negligibly small compared to the grid spacing. In reality, the laser beam diameter can be on the same size scale as the grid size. A larger laser beam diameter would lead to a smearing of the fuel concentration fluctuations across the laser beam. Thus, some of the spatial fluctuations will be averaged out across the beam of the laser. For this reason the use of focusing optics is desirable for making the diameter of the laser beam smaller than the grid size, where the grid is smaller than the Taylor scale (Hinze, 1975 [30]), at the measurement location.

Reconstruction of RMS with GAs Using LES Results

When using a GA for the reconstruction scheme, making the transition from reconstructing the mean concentration field to reconstructing the RMS concentration field involved replacing equations of the form given in Eq. (6) with equations relating the RMS concentration values to the time-dependent LOS measurements (such as equations of the form given in Eq. (11) or Eq. (15), with no further modifications to the reconstruction scheme.

The large eddy simulation (LES) was applied to modeling of the mixing depicted in Fig. 1, where fuel is injected from a central tube into coflowing air. The LES output consisted of a full concentration field resolved in time. We then imagined a laser beam probing through the concentration field generated by the LES, just as was done in the actual experiment. The RMS reconstruction algorithm has been applied to the LES time series data as a test of the performance of the RMS reconstruction technique. Projections from the LES concentration field were calculated at many time steps (time steps are 25 microseconds apart) to obtain the mean and RMS projections. The RMS projections were applied to the reconstruction algorithm, first assuming no correlation, then again assuming complete correlation. The generated concentration fields for these two cases are then compared to the original RMS concentration field that the LES model produced. This procedure is summarized in Table 3. The LES output has 47 grids in the radial direction, versus 10 to 15 grids in the GA reconstruction, meaning that the LES grid size is substantially smaller than that of the GA reconstruction.

Table 3
Procedure for testing RMS reconstruction technique using LES results

Step:	Procedure:
Generate known X_{mean} and X_{RMS} values for test case.	Make fuel concentration (X) profile that fluctuates in time, generate this profile for many (say 1000) time steps. Perform statistics on these data to get X_{RMS} and X_{mean}.
Generate known mean and RMS projections.	At each of the time steps, calculate projections that would result from the concentration profile.
Generate X_{mean} and X_{RMS} profiles from the mean and RMS projections.	Use axisymmetric GA to generate X_{mean} and X_{RMS} profiles with the mean and RMS projections used as inputs.
Compare generated X_{mean} and X_{RMS} profiles with the known values.	

Figure 4 compares the RMS of fuel volume fraction generated from the LES with the reconstructed RMS of fuel volume fraction assuming no correlation and complete correlation. The conditions for the mixing problem modeled by the LES were given previously in Table 2. Figure 4 shows that the assumption of no correlation (Eq. (11)) using 10 radial grids yields reasonable results on reconstructing the RMS of the concentration for the LES model data. The importance of the grid size used in the reconstruction should be noted. The LES result shown in Fig. 4 is higher than both the assumption of complete correlation and the assumption of no correlation with 10 grids. The reason that the no correlation assumption with 10 grids is lower than the LES result in Fig. 4 is given in the following paragraph.

With a finite number of grids, the assumption of no correlation implies that there is no correlation between the grids while fluctuations in time, on a size scale below the grid size are completely correlated. The RMS result for a no correlation assumption depends on the number of grids chosen, as illustrated by Eq. (13). If a larger number of grids were used for the reconstruction, the profile of RMS of concentration would be higher using the no correlation assumption. The reconstruction assuming no correlation was repeated for 15 grids and the result is given in Fig. 4 showing the expected increasing trend. As mentioned previously, the reconstruction of the field of RMS of the concentration from time-dependent LOS absorption measurements can only be carried out with either some knowledge or some assumption concerning the correlation of temporal fluctuations in fuel concentration at various locations. The mean grid size for the 10-grid reconstruction in Fig. 4 is on the order of 2 mm. Note that the LES was performed with 47 radial grids, but concentrated near the mixing area, so that the grid size for the LES was on the order of 0.5 mm. The 10-grid no correlation result in Fig. 4 is thus based on the implicit assumption that the concentration has no correlation on length scales greater than 2 mm, while there is complete correlation on length scales at and below 2 mm. From the LES output, the contribution of correlation to the RMS of each projection was calculated, estimated as the right hand term of Eq. (14), and was found to account for approximately 30% of the projection RMS values, roughly accounting for the underestimation of the no correlation assumption with 10 grids shown in Fig. 4.

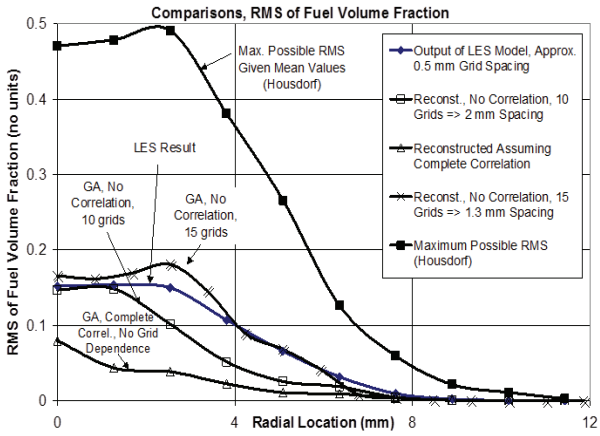

Fig. 4. RMS of fuel volume fraction generated from LES along with the reconstructed RMS of fuel volume fraction assuming no correlation, and assuming complete correlation. Additionally the maximum possible RMS profile for the problem using the Housdorf inequality is shown.

If we continued decreasing the grid size for the no correlation assumption, the reconstructed concentration RMS values will increase and would approach infinity. As the grid size decreased, eventually the no correlation assumption would no longer be accurate. At the Taylor scale (Hinze, 1975 [30]) and below, there would be correlation between grids – nearby grids would be correlated while grids that are far apart would not be correlated. Thus, there will be a maximum number of grids that could be reasonably used in performing the reconstruction with a no correlation assumption. There are two ways to represent the information regarding the correlation at small grid sizes. The first option is to select a finite number of grids where the mean grid size is selected to be somewhere near the Taylor scale for the given problem (as was done for the no correlation

assumption shown in Fig. 4). The second option is to go to smaller grid sizes, below the Taylor scale, and include correlation terms among nearby neighbor grids in the relation (an assumption in applying Eq. (10) that is between the assumption of no correlation and that of complete correlation). The approach including some correlation terms (we will call the Taylor scale correlation approach) could be set up such that the solution is independent of grid size, and therefore this approach would be more robust than the no correlation assumption approach.

As mentioned in the previous paragraph, the result of a reconstruction of the fuel concentration RMS assuming no correlation will become infinity according to Eq. (13) if the grid size decreases to zero. Some assumption about the length scale of correlations must be made, such as the dependence of correlation on Taylor length scale, so that the solution becomes independent of the number of grids. We can modify the general relation (Eq. (10)) to include one possible form of the Taylor scale correlation assumption as

$$\overline{\left[\ln\left(\frac{I_N}{I_o}\right)\right]'^2} = \alpha^2 \bullet P^{*2} \bullet \sum_{i=1}^{N} \Delta\ell_i^{\,2} \bullet \overline{X_i'^2} + \alpha^2 \bullet P^{*2} \bullet \sum_{i=1}^{N} \sum_{j=1, i\neq j}^{N} \Delta\ell_i \bullet \Delta\ell_j \bullet \left(\overline{X_i' \bullet X_j'}\right) \bullet G_{i,j} \tag{17}$$

where $G_{i,j}$ is named the "Girard factor," ranging from zero to one with no units. $G_{i,j}$ is a function of the distance between grids i and j, $D_{i,j}$, as follows:

$G_{i,j} \rightarrow 1$ when $D_{i,j} <<$ Taylor length

$G_{i,j} \rightarrow ½$ when $D_{i,j} \approx$ Taylor length

$G_{i,j} \rightarrow 0$ when $D_{i,j} >>$ Taylor length

Consequently, $\overline{\left[\ln\left(\frac{I_N}{I_o}\right)\right]'^2}$ will be independent of the grid size as long as the grid size is small enough to resolve most spatial changes in fluctuations.

The Taylor length is an estimated distance, below which correlations become substantial. A reconstruction based on Eq. (17) gives a correct reconstruction of the fuel concentration RMS for the LES data when the Taylor scale is estimated as 1.5 mm as shown in Fig. 5. The values of $G_{i,j}$ used in applying Eq. (17) were found manually for each set of grids for the result seen in Fig. 5. The values of $G_{i,j}$ were entered manually for each set of grid pairs such that when $D_{i,j}$ was less than 1 mm, $G_{i,j}$ was set to 1, when $D_{i,j}$ was between 1 mm and 2 mm, $G_{i,j}$ was set to 1/2, and when $D_{i,j}$ was greater than 2 mm, $G_{i,j}$ was set to 0. Thus, grids that are spaced less than 1.5 mm apart have correlation terms, while grids that are separated by distances much larger than 1.5 mm are not correlated in the reconstruction.

The Housdorf relation (Dimotakis and Miller, 1990 [34]) allows one to generate the maximum possible value of the RMS from a given mean. The Housdorf relation used for the maximum possible RMS is given by

$$X_{RMS} \leq \left[\overline{X} \bullet \left(1 - \overline{X}\right)\right]^{\frac{1}{2}} \tag{18}$$

Thus

$$X_{RMSMax} = \left[\overline{X} \bullet \left(1 - \overline{X}\right)\right]^{\frac{1}{2}} \tag{19}$$

where X_{RMSMax} is the maximum possible value for the fuel concentration RMS. Regardless of what information is known about the time-dependent fluctuations of the fuel volume fraction, the Housdorf relation can be used as the upper limit on the fuel concentration RMS. The maximum possible RMS profile from the Housdorf inequality (Dimotakis and Miller, 1990 [34]) for the situation is plotted in Fig. 4.

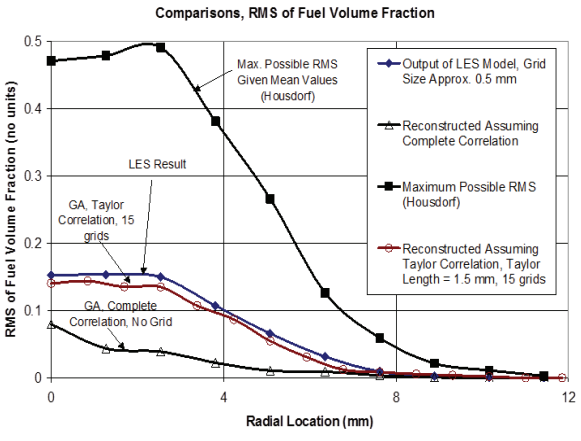

Fig. 5. RMS of fuel volume fraction generated from LES along with the reconstructed RMS of fuel volume fraction assuming Taylor scale correlation with the Taylor scale estimated as 1.5 mm. For comparison, the bounds on the RMS reconstruction are also included. The lower bound is given by assuming complete correlation. The upper bound is given from the Housdorf inequality.

Comparisons of LES VS. Experiment

Velocity measurements by hot wire anemometry were performed for an air jet into coannular air and compared with the LES model results. One set of velocity profiles is presented in Fig. 6 at $x/d = 24$, where x is axial distance and d is the diameter of the inner pipe. The velocity profile predicted by the model agrees reasonably well with the measured velocity profiles. The extent of agreement between the experiment and the LES results is not surprising as the experimentally determined mean velocity profile was used as a boundary condition in the LES.

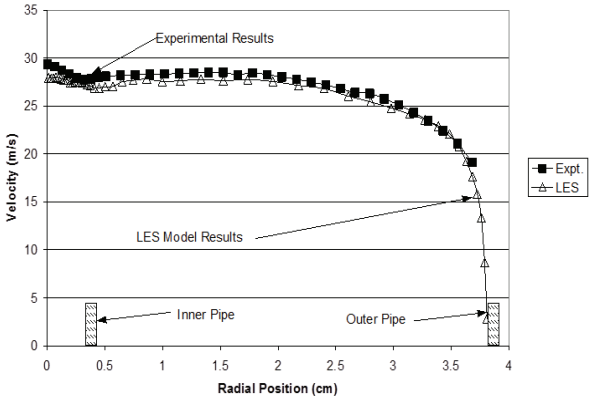

Fig. 6. Time-averaged radial velocity profiles at $x/d = 24$ for coannular pipe flow mixing experiments, air jet into air coflow. Measurements were performed with a hot wire anemometer.

As an additional check on the ability of the GAs to correctly generate the time-averaged and RMS fuel concentrations from LOS measurements, independent measurements were performed using an extractive laser probe. This instrument, called a Real-time Fuel-air Analyzer (RFA), continuously extracts a sample of gas from the desired location through a small diameter (d = 860 μm) probe at a high velocity to the instrument, where fuel concentration is measured by IR laser absorption. Because of the high velocity of the sample gas through the probe, the instrument can resolve concentration fluctuations occurring at frequencies less than ~ 600 Hz. Thus, the instrument is used in obtaining measurements, resolved in space, of not only the time-averaged concentration profile, but also of the RMS concentration profile based on turbulence fluctuations occurring below 600 Hz. More information on this instrument can be found in Girard et al. (2001 [4], 2002 [35] and in the Doctoral Thesis of Girard, 2003 [33]).

Figure 7 presents the time-averaged results of the concentration measurements made with the RFA instrument with methane as the fuel. Also plotted is the reconstructed mean profile using GAs with LOS measurements and the LES predictions. These results are for measurements taken at $x/d = 24$. As can be seen from Fig. 7, both the LES model and the GA reconstruction give results in satisfactory agreement with the experimentally measured time-averaged concentration profiles.

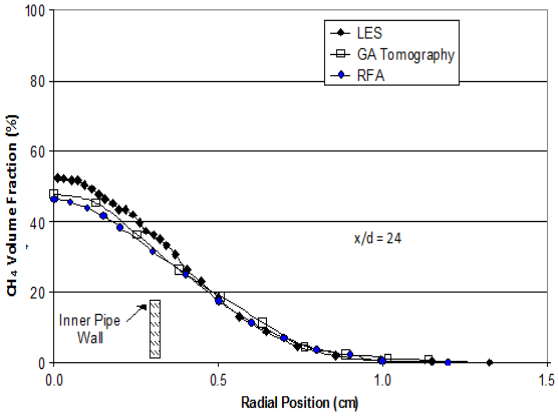

Fig. 7. Comparison of time-averaged concentration profiles: reconstructed result from LOS measurements, LES output and point measurements using RFA instrument, $x/d = 24$.

Figure 8 presents the results of the LES prediction versus experiment for two additional axial locations with methane as the fuel. From Fig. 8, one can see that the LES model results agree with experiment reasonably well.

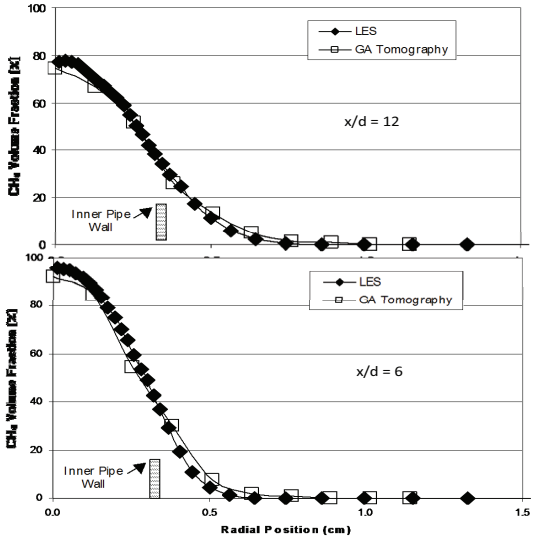

Fig. 8 Time-averaged results of LES model versus experiment for various mixing lengths for methane.

Figure 9 shows a comparison of concentration RMS versus radial position from the GA program based on experimental LOS intensity ratios, and from the LES model predictions. The reconstruction results plotted in Fig. 9 were performed with the Taylor scale estimated as 1.5 mm. This value was used based on the previous results from the LES model for the flow conditions of the coannular pipe flow experiment.

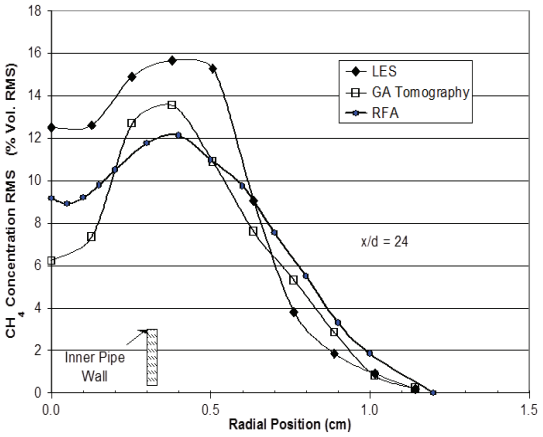

Fig. 9. RMS of methane concentration, LES versus GA (experimental) and point measurements using RFA instrument, $x/d = 24$.

Also shown in Fig. 9 are the measurements from the RFA instrument. As can be seen from Fig. 9, the RMS values obtained by the two methods (LES and GA reconstruction) follow the same trend as the RFA results, giving the same radial location of peak RMS, and the same trends versus radial location. The GA reconstruction gives better agreement with the RFA results than does the LES model. The GA reconstruction results had deviations near the centerline, as well as at the peak. The LES model overpredicts the RMS values overall (deviation of about 30% averaged by radial location) but follows the correct trends.

For the laser and optical setup employed in these experiments the beam diameter at the measurement location was 2.2 mm – defined as the diameter of the beam containing 86% of the laser power (Saleh and Teich, 1991 [36]). Thus, some smearing of the actual fluctuations of fuel concentration would occur, causing the measured signal RMS to be lower than what is really there (thus while temporal resolution was adequate, spatial resolution was marginal). By using an optical system that focuses the beam at the measurement point (Saleh and Teich, 1991 [36]), the resolution of the measurements for finding the RMS of the concentration would be improved. Nonetheless, the agreement of both the LES model and the GA reconstruction with the RFA results is satisfactory.

Conclusions

A genetic algorithm (GA) based tomographic reconstruction program has been developed to reconstruct both the time average and (for the first time) the RMS of fuel concentration from time-dependent line of sight (LOS) absorption measurements. The GA-based tomography program is successful at reproducing the time-averaged radial concentration profile from line of sight absorption measurements. The GA reconstruction of concentration RMS requires some knowledge or some assumption concerning the correlation of temporal fluctuations in fuel concentration at various locations. A correlation based on Taylor length scale is proposed and gives quantitatively correct results. The LES model predicts the extent of mixing versus downstream location well (agreement to within a radial location-based average of 5%) based on the time-averaged concentration profiles. The LES model over-predicts the RMS concentration profile generally by about 30% versus the reconstructed RMS concentration profile. The difference may be in part due to uncertainties in the RMS reconstruction and in part to the finite diameter of the laser beam.

Acknowledgments

The authors wish to thank the Department of Energy's Advanced Gas Turbine Systems Research Program for providing the funding for this research.

References

[1]. T.F. Fric, J. Propul. Power, 9 (5) (1993) 708–713.
[2]. D.P. Graham, and K. McKindley, 2nd European Conference on Industrial Furnaces and Burners (INFUB 2), Algarave, Portugal, April 2-5 (1991).
[3]. J. Warnatz, U. Maas, R.W. Dibble, Combustion, Physical and Chemical Fundamentals, Modeling and Simulation, Experiments, Pollutant Formation (3rd ed), Springer, Berlin (2001).
[4]. J.W. Girard, R.W. Dibble, L.O. Arellano, K.O. Smith, Proceedings of the ASME TURBO EXPO, Paper 2001-GT-0372 (2001).
[5]. R. Mongia, R.W. Dibble, J. Lovett, ASME Paper 98-GT-304, International Gas Turbine and Aeroengine Congress and Exposition (1998).

[6]. L.A. Shepp, and B.F. Logan, IEEE Trans. Nucl. Sci. NS-21:228 (1974).
[7]. T. Sunagawa, M. Ochi, O. Ishida, C. Ono, Y. Ikuta, J. Computer Assisted Tomography, 27 (3) (2003)169–174.
[8]. G.W. Faris, Quantitative Optical Tomographic Imaging of Fluid Flows and Flames, Ph.D. Dissertation, Stanford University (1986).
[9]. S.J. Carey, H. McCann, D.E. Winterbone, and E. Clough, 1st World Congress on Industrial Process Tomography, Buxton, Greater Manchester, April 14-17 (1999).
[10]. M. Bertero, and P. Boccacci, Introduction to Inverse Problems in Imaging, IOP, Bristol, U.K (1998).
[11]. R.A. Williams, and M.S. Beck, Eds., Process Tomography – Principles, Techniques and Applications, Butterworth-Heinemann Ltd, Oxford, U.K (1995).
[12]. S.B. Pope, Turbulent Flows, Cambridge University Press, Cambridge, UK (2000).
[13]. N. Branley, and W.P. Jones, Combust. Flame 127 (2001) 1914–1934.
[14]. H. Forkel, Uber die Grobstruktursimulation Turbulenter Wasserstoff-Diffussionsflammen, Ph.D. Dissertation, Technische Universitat Darmstadt (1999).
[15]. H. Forkel, and J. Janicka, in: 1st Int. Symposium on Turbulence and Shear Flow Phenomena, Santa Barbara, CA, USA, September 12-15 (1999).
[16]. A. Kemp, H. Forkel, J.-Y. Chen, A. Sadiki, J. Janicka, Proc. Comb. Inst., 28 (2001) 35–40.
[17]. M. Germano, U. Piomelli, P. Moin, W.H. Cabot, Phys. Fluids A, 3 (1991) 1760–1765.
[18]. F. White, Fluid Mechanics, (3rd ed), McGraw Hill, New York (1994).
[19]. J.G. Lee, K. Kim, D.A. Santavicca, Proc. Comb. Inst. 28: Pub. No. 2D03 (2000).
[20]. S. Yoshiyama, Y. Hamamoto, E. Tomita, K. Minami, JSAE Review, 17 (1996) 339–345.
[21]. M.Y. Perrin, and J.M. Hartmann, J. Quant. Spect. Rad. Trans., 42 (6) (1989) 459–464.
[22]. R. Mongia, Optical Probe for Measuring the Extent of Air and Fuel Mixing in Lean Premixed Combustors and the Effect of Air & Fuel Mixing on Combustor Performance, Ph.D. Dissertation, U. of California, Berkeley (1998).
[23]. V. Ebert, T. Fernholz, C. Geisemann, H. Pitz, H. Teichert, J. Wolfrum, Proc. Comb. Inst. 28: Pub. No. 2D04 (2000).
[24]. N.H. Abel, J. Reine Angew. Math. 1 (1826) 153–157.
[25]. C.J. Dasch, Appl. Opt. 31 (8) (1992) 1146–1152.
[26]. M. Ravichandran, and F.C. Gouldin, Appl. Opt., 27 (19) (1988) 4084–4097.
[27]. A.K. Jain, Fundamentals of Digital Image Processing Design, Prentice Hall, NJ (1989).
[28]. K.D. Kihm, and D.P. Lyons, Opt. Lett. 21 (17) (1996) 1327–1329.
[29]. J. Kybic, T. Blu, and M. Unser, "Variational Approach to Tomographic Reconstruction," Proceedings of SPIE Medical Imaging, San Diego (2001).
[30]. J.O. Hinze, Turbulence (2nd ed.), McGraw Hill, New York, Sec. 6.8 (1975).
[31]. D. Goldberg, Genetic Algorithms in Search, Optimization, and Machine Learning, Addison Wesley, NY (1989).
[32]. D. Powell, M.M. Skolnick, Proc. Fifth Int. Conf. Genetic Algorithms (1993).
[33]. J.W. Girard, The Application of Laser Diagnostics, Light Emitting Diodes and Computer Modeling to the Characterization of Fuel-Air Mixing in High Pressure Lean Premixed Combustion Systems, Ph.D. Dissertation, U. of California, Berkeley (2003).
[34]. P.E. Dimotakis and P.L. Miller, Phys. Fluids A, 2 (11) (1990) 1919–1920.
[35]. J.W. Girard, R.W. Dibble, D.L. Flowers, S.M. Aceves, SAE Paper No. 2002-01-1758 (2002).
[36]. B.E.A. Saleh, M.C. Teich, Fundamentals of Photonics, John Wiley & Sons (1991).

Received 4 March 2014